# Numerical study of photoinduced dynamics in a double-exchange model

Y. Kanamori,[1] H. Matsueda,[2] and S. Ishihara[1,3]
[1]*Department of Physics, Tohoku University, Sendai 980-8578, Japan*
[2]*Sendai National College of Technology, Sendai 989-3128, Japan*
[3]*Core Research for Evolutional Science and Technology (CREST), Tsukuba 305-0047, Japan*
(Received 19 April 2010; revised manuscript received 25 June 2010; published 1 September 2010)

Photoinduced spin and charge dynamics in double-exchange model are numerically studied. The Lanczos method and the density-matrix renormalization-group method are applied to one-dimensional finite-size clusters. By photon irradiation in a charge-ordered (CO) insulator associated with antiferromagnetic (AFM) correlation, both the CO and AFM correlations collapse rapidly, and appearances of new peaks inside of an insulating gap are observed in the optical spectra and the one-particle excitation spectra. Time evolutions of the spin correlation and the in-gap state are correlated with each other, and are governed by the transfer integral of conduction electrons. Results are interpreted by the charge kink/antikink picture and their effective motions which depend on the localized spin correlation. Pump-photon density dependence of spin and charge dynamics are also studied. Roles of spin degree of freedom are remarkable in a case of weak photon density. Implications of the numerical results for the pump-probe experiments in perovskite manganites are discussed.

DOI: 10.1103/PhysRevB.82.115101 PACS number(s): 71.30.+h, 78.47.J−, 78.20.Bh, 71.10.−w

## I. INTRODUCTION

Coherent controlling of electronic and structural phases by shining light has been one of the attractive themes not only in fundamental condensed-matter physics but also in electric and communication technologies. Drastic state change by photon irradiation, often termed photoinduced phase transition, is ubiquitously seen in a variety of materials.[1,2] In particular, a number of studies in photoirradiation effects have been done in correlated electron systems, such as transition-metal oxides, low-dimensional organic salts, and others. This is because (i) cooperative and ultrafast changes in states by light occur due to strong electron correlation and (ii) coupling between multiple degrees of freedom of electron, i.e., spin, charge, and orbital, exhibits a variety of photoinduced phenomena. In recent rapid progresses of experimental techniques, transient and nonequilibrium states induced by light irradiation have been examined by several kinds of time-resolved scattering and spectroscopy experiments, for example, photoemission spectroscopy,[3] x-ray diffraction,[4,5] electron diffraction,[6] and so on in addition to the conventional optical pump-probe spectroscopy.

Perovskite manganites $R_{1-x}A_xMnO_3$ ($R$: a rare-earth ion, $A$: an alkaline-earth ion) is one of the well-studied correlated electron materials in a viewpoint of ultrafast photoinduced phenomena. A nominal valence of a Mn ion is $3+x$ and the electron configuration of the $3d$ orbitals is $d^{4-x}$. One of the doubly degenerate $e_g$ orbitals is occupied by $1-x$ electron and the $t_{2g}$ orbitals are occupied by three electrons with parallel spin. One remarkable property in manganite is strong phase competition. Around $x=0.5$, a subtle energy balance controls stability of two electronic phases; charge ordered (CO) insulator associated with antiferromagnetic (AFM) order and ferromagnetic (FM) metal.[7] Colossal magnetoresistance (CMR) effect is one of the examples of drastic phase change between the two phases by applying external field.[8] Electronic and structural phase controlling is also performed by light.[9–19] By photoirradiation in CO insulating phase, the optical-absorption spectra around the charge-transfer excitation shift to lower energy.[11] After 10 ns, the spectra are almost recovered. These experimental results imply a generation of a transient metallic state by photoirradiation and its fast relaxation within 10 ns. The transient magnetic property was examined by the magneto-optical Kerr spectroscopy. A Kerr rotation appears by photoirradiation and its angle gradually increases within 1 ps.[13,15,17] That is, to say, spin and charge structures are changed cooperatively by pump-photon irradiation. The excitation density dependence of the photoinduced state was also examined in the pump-probe experiments.[16] The results provide a clue to resolve a stability of the photoinduced FM metal and its relaxation mechanism.

Theoretical study of manganites has been done mainly from the view point of origin of CMR. The double-exchange (DE) model is not only studied as a model for manganites but also recognized to be a standard theoretical model in solid-state physics.[20–23] In this model, conduction electrons corresponding to the $e_g$ electrons couple ferromagnetically with localized spins for the $t_{2g}$ spins. A number of theoretical calculations of the optical and transport properties in the DE model have been already carried out. On the contrary, transient and nonequilibrium properties in the DE model are very limited so far.

In this paper, motivated from the optical pump-probe experiments in perovskite manganites, we present a numerical study of the photoinduced dynamics in the one-dimensional DE model. Time dependences of the static and dynamical quantities are calculated by applying the Lanczos method and the density-matrix renormalization-group (DMRG) method in finite-size clusters. By photoirradiation in the CO and AFM insulating phase, both the CO and AFM correlations rapidly collapse. New peak structures appear inside of the gap in the optical-absorption spectra and the one-particle excitation spectra, and grow up with time. It is shown that time dependences of the spin correlation and the new peak structures are scaled by a universal curve. This implies strong coupling between the charge and spin sectors in tran-

 

sient photoexcited state. We also study the pump-photon density dependence of the photoinduced dynamics. Roles of spin degree are remarkable in a region of weak photon density in comparison with charge degree. Implications of the present numerical calculations for the photoinduced phenomena in manganites are discussed.

In Sec. II, the extended DE model and a formulation of the photoexcited states are presented. The numerical methods applied to one-dimensional clusters are introduced in Sec. III. The ground-state properties before photoirradiation are briefly introduced in Sec. IV. The main part in this paper is Sec. V where the numerical results for the photoinduced spin and charge dynamics are presented. The pump-photon density dependences of the photoinduced dynamics are shown in Sec. VI. Section VII is devoted to discussion and concluding remarks. Details of an effective model and analytical results in the spinless *V-t* model are given in the Appendix. A part of this paper was briefly presented in Ref. 24.

## II. MODEL AND FORMULATION

We introduce the one-dimensional extended DE model to examine both the CO insulating state associated with the AFM order and the FM metallic state. A model Hamiltonian is given by

$$\mathcal{H}_0 = -\alpha t \sum_{\langle ij\rangle\sigma} (c_{i\sigma}^\dagger c_{j\sigma} + \text{H.c.}) + U\sum_i n_{i\uparrow}n_{i\downarrow} + V\sum_{\langle ij\rangle} n_i n_j - J_H\sum_i \sum_i \boldsymbol{S}_i\cdot\boldsymbol{s}_i + J_S\sum_{\langle ij\rangle}\boldsymbol{S}_i\cdot\boldsymbol{S}_j, \quad (1)$$

where $c_{i\sigma}$ is the annihilation operator for a conduction electron with spin $\sigma(=\uparrow,\downarrow)$ at site $i$, and $\boldsymbol{S}_i$ is a spin operator for the localized spin. We introduce the number operator $n_i = \Sigma_\sigma n_{i\sigma} = \Sigma_\sigma c_{i\sigma}^\dagger c_{i\sigma}$ and the spin operator $\boldsymbol{s}_i = (1/2)\Sigma_{\alpha\beta} c_{i\alpha}^\dagger(\boldsymbol{\sigma})_{\alpha\beta} c_{i\beta}$ with the Pauli matrices $\boldsymbol{\sigma}$ for the conduction electrons. The first term in Eq. (1) is for the electron hopping with amplitude $\alpha t$ between the nearest-neighboring (NN) sites. The second and third terms represent the on-site Coulomb interaction $U$, and the NN Coulomb interaction $V$ for the conduction electrons, respectively. We consider the Hund coupling $J_H(>0)$ between the conduction electron and the localized spin, and the AFM superexchange interaction $J_S(>0)$ between the NN localized spins. We take $t=1$ as a unit of energy, and a magnitude of the transfer integral is changed by changing the parameter $\alpha$. For simplicity, we assume a single orbital for a conduction electron and $S=1/2$ for a localized spin.

The vector potential for the pump photon at time $\tau$ is given as $\boldsymbol{A}_{\text{pump}}(\tau) = A_{\text{pump}}(\tau)\hat{z}$, where the $z$ axis is taken to be parallel to the chain direction. The interaction between the conduction electrons and the pump photon is introduced as the Peierls phase,

$$\mathcal{H}'(\tau) = -\alpha t \sum_{\langle ij\rangle\sigma} c_{i\sigma}^\dagger c_{j\sigma}\left[e^{-i\int \boldsymbol{A}_{\text{pump}}(\tau)\cdot d\boldsymbol{r}} - 1\right] + \text{H.c.}, \quad (2)$$

where a subtraction in the parenthesis corresponds to the first term in Eq. (1). In a case of weak pump-photon density, this Hamiltonian is reduced into the following form:

$$\mathcal{H}'(\tau) = -jA_{\text{pump}}(\tau), \quad (3)$$

up to the order of $O(A_{\text{pump}})$. We introduce the current operator defined by $j = i\alpha t\Sigma_{\langle ij\rangle\sigma}(c_{i\sigma}^\dagger c_{j\sigma} - \text{H.c.})$. By using the first-order time-dependent perturbation theory with respect to $\mathcal{H}'(\tau)$, the wave function at time $\tau$ is obtained as

$$|\phi_0(\tau)\rangle = e^{-iE_0\tau}|0\rangle + \sum_{n\neq 0} c_n(\tau)|n\rangle, \quad (4)$$

where a coefficient is given by

$$c_n(\tau) = ie^{-iE_n\tau}\langle n|j|0\rangle\int_{-\infty}^{\tau} d\tau' A_{\text{pump}}(\tau')e^{-i(E_0-E_n)\tau'}, \quad (5)$$

and $|n\rangle$ is the $n$th eigenstate of $\mathcal{H}_0$ with the energy $E_n$. We assume that the system is in the ground state $|0\rangle$ at $\tau=-\infty$. Since the first term in Eq. (4) shows the trivial time evolution due to the phase factor, we focus on the second term which represents the one-photon absorbed state. Several transient physical quantities introduced below correspond to the differences between the data before and after pump-photon irradiation. From now on, this is termed $|\phi(\tau)\rangle$ as

$$|\phi(\tau)\rangle \equiv \sum_{n\neq 0} c_n(\tau)|n\rangle. \quad (6)$$

The vector potential for the pump photon is assumed to be a damped oscillator form as

$$A_{\text{pump}}(\tau) = A_1 \exp(-\gamma_0|\tau| - i\omega_0\tau), \quad (7)$$

where $\omega_0$ is a frequency and $\gamma_0$ is a damping factor. We impose a condition of $\tau \gg \gamma_0^{-1}$ which implies that the pump photon is fully damped at time $\tau$ of our interest. Then, the coefficient in Eq. (5) is obtained as

$$c_n(\tau) = iA_1 e^{-iE_n\tau}\langle n|j|0\rangle\int_{-\infty}^{\infty} d\tau' e^{-i(\omega_0-E_n+E_0)\tau'-\gamma_0|\tau'|} = -2iA_1 e^{-iE_n\tau}\langle n|j|0\rangle \text{Im}\left[\frac{1}{\omega_0 - E_n + E_0 + i\gamma_0}\right]. \quad (8)$$

By inserting this expression, we have the wave function at time $\tau$ as

$$|\phi(\tau)\rangle = -2iA_1\sum_{n\neq 0} e^{-iE_n\tau} \times \text{Im}\left[\frac{1}{\omega_0 - E_n + E_0 + i\gamma_0}\right]|n\rangle\langle n|j|0\rangle = -2iA_1 e^{-i\mathcal{H}_0\tau}\,\text{Im}\left[\frac{1}{\omega_0 - \mathcal{H}_0 + E_0 + i\gamma_0}\right]j|0\rangle, \quad (9)$$

where $\langle 0|j|0\rangle = 0$ is used. Here we redefine the one-photon absorbed state by

$$|\phi(\tau)\rangle = \frac{1}{\mathcal{N}}e^{-i\mathcal{H}_0\tau}\,\text{Im}\left[\frac{1}{\omega_0 - \mathcal{H}_0 + E_0 + i\gamma_0}\right]j|0\rangle \quad (10)$$

with a normalization factor $\mathcal{N}$.

Photoexcited states are monitored by calculating the several kinds of static and dynamical quantities. The transient excitation spectra are formulated based on the linear-

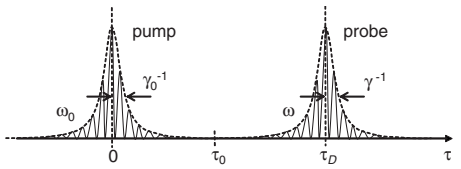


FIG. 1. A schematic view of the wave packets for the pump and probe light intensities as a function of time.

response theory. We explain, as an example, a formulation of the transient optical-absorption spectra. The vector potential for the probe photon is set to be parallel to the $z$ direction and has a damped oscillator form as $\boldsymbol{A}_{\text{probe}}(\tau)=A_{\text{probe}}(\tau)\hat{z}$ and

$$A_{\text{probe}}(\tau)=A_2\exp(-\gamma|\tau-\tau_D|-i\omega\tau) \tag{11}$$

with a frequency $\omega$, the center of an envelope $\tau_D$, and a damping factor $\gamma$. We assume that the pump photon is fully damped at time when the probe photon comes in, and there are no interference between the pump and probe photons. This is given by the condition $(\tau_D-\gamma^{-1})\gg\gamma_0^{-1}$. A schematic picture for the pump-photon and probe-photon wave packets is shown in Fig. 1. The interaction Hamiltonian between the probe photon and the conduction electrons at time $\tau$ is given by

$$\mathcal{H}''(\tau)=-jA_{\text{probe}}(\tau) \tag{12}$$

within the first order of $A_{\text{probe}}(\tau)$. When the probe photon is taken into account, the electronic wave function at time $\tau$ $(\gg\gamma_0^{-1})$ is given by

$$|\psi(\tau)\rangle=U(\tau,\tau_0)|\phi(\tau_0)\rangle. \tag{13}$$

Here, $|\phi(\tau_0)\rangle$ is the wave function at time $\tau_0$ where a condition $\tau_D-\gamma^{-1}\gg\tau_0\gg\gamma_0^{-1}$ is satisfied and is given by Eq. (10). The time-evolution operator is defined by

$$U(\tau,\tau_0)=U_0(\tau,\tau_0)U_1(\tau,\tau_0) \tag{14}$$

with

$$U_0(\tau,\tau_0)=\exp[-i\mathcal{H}_0(\tau-\tau_0)] \tag{15}$$

and

$$U_1(\tau,\tau_0)=P\exp\left[i\int_{\tau_0}^{\tau}d\tau' j(\tau',\tau_0)A_{\text{probe}}(\tau')\right], \tag{16}$$

where $P$ is the time-ordered operator and $j(\tau',\tau_0)$ $[=U_0^{\dagger}(\tau',\tau_0)jU_0(\tau',\tau_0)]$ is the interaction representation of the current operator. The expectation value of the current operator at time $\tau$ is given as

$$\begin{aligned}\langle j\rangle(\tau)&\equiv\langle\psi(\tau)|j|\psi(\tau)\rangle\\&=-i\int_{\tau_0}^{\tau}d\tau'\langle\phi(\tau_0)|[j(\tau',\tau_0),j(\tau,\tau_0)]|\phi(\tau_0)\rangle A_{\text{probe}}(\tau')\\&\quad+\mathcal{O}(A_{\text{probe}}^2).\end{aligned} \tag{17}$$

Here we use a relation $\langle\phi(\tau_0)|j(\tau,\tau_0)|\phi(\tau_0)\rangle=0$ because $|\phi(\tau)\rangle$ is an eigenstate of parity. By inserting the complete set into the integrand and integrating out $\tau'$ under the condition of $(\tau_D-\tau_0)\gg\gamma^{-1}$, we obtain

$$\langle j\rangle(\tau)=\chi(\omega,\tau)A_{\text{probe}}(\tau)+\chi_0(\omega,\tau)A_{\text{probe}}(\tau_D) \tag{18}$$

with

$$\chi(\omega,\tau)=-\sum_{nml}\bar{c}_n^*(\tau)\bar{c}_l(\tau)j_{nm}j_{ml}\times\left[\frac{1}{\omega-E_m+E_l\pm i\gamma}-\frac{1}{\omega-E_n+E_m\pm i\gamma}\right] \tag{19}$$

and

$$\chi_0(\omega,\tau)=-\theta(\tau-\tau_D)2i\gamma\sum_{nml}j_{nm}j_{ml}\times\left[\frac{\bar{c}_n^*(\tau)\bar{c}_l(\tau_D)e^{-iE_m(\tau-\tau_D)}}{(\omega-E_m+E_l)^2+\gamma^2}-\frac{\bar{c}_n^*(\tau_D)\bar{c}_l(\tau)e^{iE_m(\tau-\tau_D)}}{(\omega-E_n+E_m)^2+\gamma^2}\right]. \tag{20}$$

We introduce $\bar{c}_n(\tau)=\langle n|\phi(\tau)\rangle$ which is proportional to $c_n(\tau)$ in Eq. (8), and $j_{nm}=\langle n|j|m\rangle$. The first and second terms in Eq. (18) represent the induced current which is proportional to the probe-photon vector potential $A_{\text{probe}}(\tau)$, and the oscillating part which remains to be finite at $\tau=+\infty$, respectively. The positive and negative signs of $i\gamma$ in the denominators of Eq. (19) are for the cases of $\tau<\tau_D$ and $\tau>\tau_D$, respectively. We focus on the first term in Eq. (18) with the positive sign of $i\gamma$ in $\chi(\omega,\tau)$, from now on. The first and second terms in $\chi(\omega,\tau)$ represents the photon-absorption and photon-emission processes, respectively. The optical-absorption spectra is defined by the imaginary part of the first term given as

$$\alpha(\omega,\tau)=-\frac{1}{L\pi}\text{Im}\sum_{nml}\frac{\bar{c}_n^*(\tau)\bar{c}_l(\tau)j_{nm}j_{ml}}{\omega-E_m+E_l+i\gamma}, \tag{21}$$

where $L$ is the system size.

In the similar way, the one-particle excitation spectra are obtained as a sum of the electron and hole parts: $A(q,\omega)=A^{\text{hole}}(q,\omega)+A^{\text{ele}}(q,\omega)$ with

$$A^{\text{hole}}(q,\omega)=\sum_{nml\sigma}\text{Im}\frac{\bar{c}_n^*(\tau)\bar{c}_l(\tau)\langle n|c_{q\sigma}|m\rangle\langle m|c_{-q\sigma}^{\dagger}|l\rangle}{-\pi(\omega-E_m+E_l+i\gamma)} \tag{22}$$

and

$$A^{\text{ele}}(q,\omega)=\sum_{nml\sigma}\text{Im}\frac{\bar{c}_n^*(\tau)\bar{c}_l(\tau)\langle n|c_{q\sigma}^{\dagger}|m\rangle\langle m|c_{-q\sigma}|l\rangle}{-\pi(-\omega-E_m+E_l+i\gamma)}. \tag{23}$$

We also obtain the imaginary part of the dynamical charge susceptibility as

$$N(q,\omega)=-\frac{1}{\pi}\sum_{nml}\bar{c}_n^*(\tau)\bar{c}_l(\tau)\langle n|n_q|m\rangle\langle m|n_{-q}|l\rangle\times\text{Im}\left[\frac{1}{\omega-E_m+E_l+i\gamma}-\frac{1}{\omega-E_n+E_m+i\gamma}\right] \tag{24}$$

and that of the dynamical spin susceptibility for the localized spin as

$$S(q,\omega) = -\frac{1}{\pi}\sum_{nml} \bar{c}_n^*(\tau)\bar{c}_l(\tau)\langle n|\boldsymbol{S}_q|m\rangle\langle m|\boldsymbol{S}_{-q}|l\rangle \times \mathrm{Im}\left[\frac{1}{\omega - E_m + E_l + i\gamma} - \frac{1}{\omega - E_n + E_m + i\gamma}\right], \tag{25}$$

where $c_{q\sigma}$, $n_q$, and $\boldsymbol{S}_q$ are the Fourier transforms of $c_{i\sigma}$, $n_i$, and $\boldsymbol{S}_i$, respectively.

In the numerical calculation, to reduce the computer resource, $E_n$ and $E_l$ in the denominator of Eq. (19) are replaced by the expectation value for $\mathcal{H}_0$ with respect to the wave function after the pump irradiation, i.e., $E_p = \langle\phi(\tau)|\mathcal{H}_0|\phi(\tau)\rangle$. Then the response function is rewritten as

$$\chi(\omega,\tau) \simeq -\langle\phi(\tau)|j\left[\frac{1}{\omega - \mathcal{H}_0 + E_p + i\gamma} - \frac{1}{\omega - E_p + \mathcal{H}_0 + i\gamma}\right] \times j|\phi(\tau)\rangle. \tag{26}$$

The same approximation is applied to the optical-absorption spectra and the one-particle excitation spectra. This approximation is reasonable in the present case where the pump-photon energy is tuned around a narrow energy region of $\omega_0 \pm \gamma_0$ with $\gamma_0 \ll \omega_0$. We have numerically confirmed in the calculation of $\alpha(\omega)$ that this approximation reproduces quantitatively the results based on the exact expression in Eq. (21). In order to unify the expressions before and after pumping, we introduce the following expression for the optical absorption spectra:

$$\alpha(\omega) = -\frac{1}{L\pi}\mathrm{Im}\left\langle j\frac{1}{\omega - \mathcal{H}_0 + \langle\mathcal{H}_0\rangle + i\gamma}j\right\rangle. \tag{27}$$

A bracket $\langle\cdots\rangle$ implies the expectation value with respect to $|0\rangle$ before pumping, and that with respect to $|\phi(\tau)\rangle$ after pumping.

## III. METHOD

In order to analyze the photoexcited states in the generalized DE model, the ED method based on the Lanczos algorithm and the DMRG method[25–29] are applied into one-dimensional finite-size clusters.

In the ED method, one-photon absorbed state at $\tau=0$ is calculated by inserting a subset $\{|\tilde{n}\rangle\}$ with finite dimension $M_1$, instead of the complete set $\{|n\rangle\}$, in Eq. (10) as

$$|\phi(\tau=0)\rangle \simeq \frac{1}{\mathcal{N}}\sum_{\tilde{n}}^{M_1}\mathrm{Im}\left[\frac{\langle\tilde{n}|j|0\rangle}{\omega_0 - E_{\tilde{n}} + E_0 + i\gamma_0}\right]|\tilde{n}\rangle. \tag{28}$$

This set of the wave functions is obtained by the Lanczos procedure with the $M_1$ steps from a trial function $j|0\rangle$, and $E_{\tilde{n}}$'s are the corresponding eigenenergies. We take $M_1 = 300-400$ which is enough for the optical-absorption spectra before pumping. This reduction technique is also used to calculate the time evolution of the wave function. The wave function at time $\tau+\delta\tau$ is obtained from $|\phi(\tau)\rangle$ (Ref. 30)

$$|\phi(\tau+\delta\tau)\rangle \simeq \sum_{\tilde{n}}^{M_2} e^{-iE_{\tilde{n}}\delta\tau}|\tilde{n}\rangle\langle\tilde{n}|\phi(\tau)\rangle, \tag{29}$$

where a subset with a dimension $M_2$ is obtained by the Lanczos procedure for the Hamiltonian $\mathcal{H}_0$ from the trial function $|\phi(\tau)\rangle$. We take $M_2=20$ and $\delta\tau = 10^{-2}/t - 10^{-3}/t$ which are enough for the several time-dependent quantities. We checked that the total energy remains to be a constant within an error on the order of $10^{-10}t$.

In the DMRG method, we use the multitarget DMRG algorithm to obtain the excitation spectra and the time evolution. The density matrix for the system block is set to be

$$\rho_{ii'} = \sum_{\alpha j} p^{(\alpha)}\psi_{ij}^{(\alpha)*}\psi_{i'j}^{(\alpha)}, \tag{30}$$

where $p^{(\alpha)}$ is the weight for the $\alpha$th target with a relation $\Sigma_\alpha p^{(\alpha)}=1$, $i(i')$ and $j$ represent the states in the system and environment blocks, respectively, and $\psi^{(\alpha)}$ is the wave function of the $\alpha$th target state. For the excitation spectra with respect to the operator $\mathcal{O}$ before pumping, we take the following target states:

$$\left\{|0\rangle, \mathcal{O}|0\rangle, \frac{1}{\omega - \mathcal{H}_0 + E_0 + i\gamma}\mathcal{O}|0\rangle\right\}. \tag{31}$$

For example, we take $\mathcal{O}=j$ for the optical-absorption spectra. In the calculation of the correction vector in Eq. (31), we use the reduced basis set obtained by the Lanczos procedure from the trial wave function $\mathcal{O}|0\rangle$. To obtain the wave function $|\phi(\tau)\rangle$ at time $\tau$ after pumping, we take the following target states:

$$\{|0\rangle, j|0\rangle, |\phi(\tau)\rangle\}, \tag{32}$$

where we define

$$|\phi(\tau)\rangle \simeq \frac{1}{\mathcal{N}}\sum_{\tilde{n}}^{M_3} e^{-iE_{\tilde{n}}\tau}\mathrm{Im}\left[\frac{\langle\tilde{n}|j|0\rangle}{\omega_0 - E_{\tilde{n}} + E_0 + i\gamma_0}\right]|\tilde{n}\rangle. \tag{33}$$

Here, $\{|\tilde{n}\rangle\}$ is the reduced basis set with dimension $M_3 = 300-400$ obtained by the Lanczos procedure in $\mathcal{H}_0$ from the trial function $j|0\rangle$, and $E_{\tilde{n}}$'s are the corresponding eigenenergies. We also adopt other sets of the target states, e.g., $\{|0\rangle, \phi(\tau)\rangle\}$ and $\{|0\rangle, j|\,\rangle, \phi(\tau)\rangle, \phi(\tau+\delta\tau)\rangle\}$ but the set given in Eq. (32) is the optimum choice for the numerical accuracy and the computer time consuming. We confirm that the total energy is a constant within an error on the order of $10^{-3}t$. In the calculation of the transient excitation spectra at time $\tau$, the following target states are adopted:

$$\left\{|0\rangle, j|0\rangle, |\phi(\tau)\rangle, \mathcal{O}|\phi(\tau)\rangle, \frac{1}{\omega - \mathcal{H}_0 + E_p + i\gamma}\mathcal{O}|\phi(\tau)\rangle\right\}. \tag{34}$$

The truncation number is chosen to be $m=300$ in most of the calculations, and $m=800$ in some cases. The discarded weight defined by $w = 1 - \Sigma_i^m a_i$, where $a_i$ is the eigenvalue of the density matrix, is on the order of $10^{-12}$ for the ground state, and $10^{-8}-10^{-4}$ for the photoexcited states. These are confirmed to be enough to obtain the ground-state energy within an error on the order of $10^{-3}t$ and an almost constant

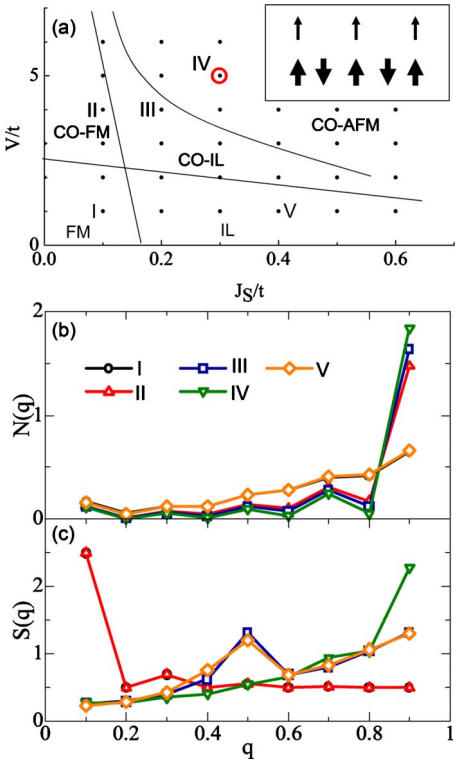


FIG. 2. (Color online) (a) Ground-state phase diagram. Dots represent the calculated points. Abbreviations CO, FM, AFM, and IL imply the charge-ordered phase, the ferromagnetic phase, the antiferromagnetic phase, and the island phase, respectively. The inset shows a schematic picture for the spin and charge configurations in the CO-AFM phase. A circle represents the parameters adopted in the numerical calculation in Secs. V and VI. (b) Charge-correlation function $N(q)$ and (c) spin-correlation function $S(q)$ for the localized spins. Symbols I–V correspond to the parameters in (a). Numerical data of $S(q)$ in I and II are almost overlapped. Other parameters are chosen to be $L=9$, $U=20t$, and $J_H=15t$.

value of the total energy in the time evolution mentioned above.

To remove boundary effects, system size $L$ is set to be odd, and a number of the conduction electrons are $N=(L+1)/2$ which correspond to the quarter filling in the open-boundary condition. This is because the charge-ordered state is not realized in the even number size cluster. We take $L=9$ and 13, and confirmed no qualitative differences between the two results. We mainly show the results in $L=9$ and $N=5$.

## IV. INITIAL STATE

First we show the electronic structure before photoirradiation. In Fig. 2(a), the phase diagram is presented in the plane of $V$ and $J_S$. This is obtained by the charge-correlation function defined by

$$N(q) = \frac{2}{L+1}\sum_{ij} \sin qr_i \sin qr_j \langle \delta n_i \delta n_j \rangle \tag{35}$$

with the charge fluctuation operator $\delta n_i = n_i - N/L$, and the spin-correlation function for the localized spin defined by

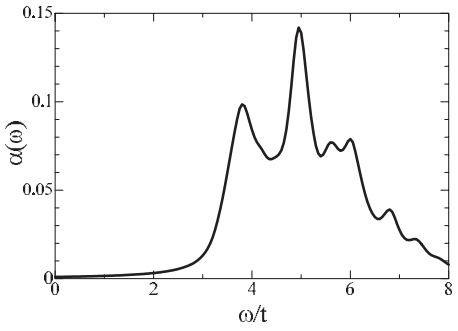


FIG. 3. Optical-absorption spectra $\alpha(\omega)$. Parameters are chosen to be $\gamma=0.2t$ and $L=9$.

$$S(q) = \frac{2}{L+1}\sum_{ij} \sin qr_i \sin qr_j \langle \boldsymbol{S}_i \cdot \boldsymbol{S}_j \rangle. \tag{36}$$

The correlation functions in each phase are shown in Figs. 2(b) and 2(c). Because of the open-boundary condition adopted in the present cluster, we introduce the quasimomentum[31] in a potential well of width $L$ defined by

$$q = \frac{n\pi}{L+1} \tag{37}$$

with an integer $n(=1,2,\ldots,L)$, and the momentum representation of a local operator $\mathcal{O}_i$ as

$$\mathcal{O}_q = \sqrt{\frac{2}{L+1}}\sum_i \mathcal{O}_i \sin qr_i, \tag{38}$$

which takes zero at $i=0$ and $L+1$. It is shown in the figures that, in the CO phase, $N(q)$ takes a sharp peak at $q=\pi$. There are three CO phases; (1) the CO-FM phase, (2) the CO island phase (CO-IL) where $S(q)$ has a weak peak, and (3) the CO-AFM phase. In the CO-AFM phase of our present interest, total spin-quantum number defined by $\vec{S}^{tot}=\Sigma_i(\vec{S}_i+\vec{s}_i)$ is $(L+3)/4$, and a correlation function between a localized spin and a conduction electron at the same site is $N^{-1}\Sigma_i\langle \boldsymbol{S}_i \cdot \boldsymbol{s}_i \rangle = 0.247$. These imply a ferrimagnetic configuration as shown in the inset of Fig. 2(a) where the conduction electrons and localized spins form the spin-triplet states at every other site. The obtained phase diagram is qualitatively consistent with the previous result in Ref. 32

The photoinduced spin and charge dynamics are examined in the CO-AFM phase near the phase boundary. A set of the parameter values are $U=20t$, $V=5t$, $J_H=15t$, and $J_S=0.3t$ which are marked by a circle in Fig. 2(a). These values are somewhat larger than the realistic values for the perovskite manganite but are required to realize the CO-AFM phase in one-dimensional clusters. The results are not sensitive to the numerical values of $U$ and $J_H$.

The optical-absorption spectra calculated in this parameter set is shown in Fig. 3. In naive sense, these optical spectra correspond to the excitations from the alternate charge configuration $\cdots 1010101 \cdots$ in a chain to the configuration $\cdots 1011001 \cdots$ where 1 and 0 represent the electron occupied and unoccupied sites, respectively. The peak structures in $\alpha(\omega)$ are explained by the charge kink/antikink pic-

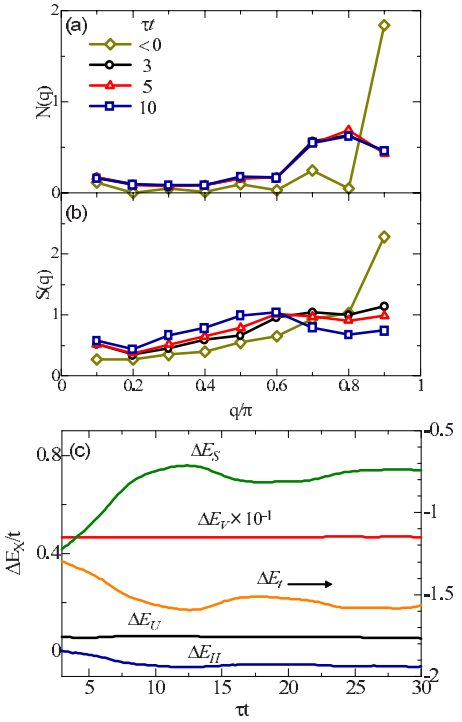


FIG. 4. (Color online) (a) Charge-correlation functions and (b) spin-correlation functions of localized spins at various times. (c) Time dependence of the difference energy for each term in the Hamiltonian $\Delta E_X$. The NN Coulomb-interaction term is scaled by 1/10.

ture which will be introduced in Sec. V B. In the next section, we focus on the photoinduced dynamics where the pump-photon energy is tuned around the edge of these spectra.

## V. PHOTOINDUCED DYNAMICS

In this section, we introduce the numerical results for the photoinduced dynamics. The pump energy is tuned at the lowest peak in $\alpha(\omega)$ in Fig. 3, i.e., $\omega_0=3.8t$ with a damping constant $\gamma_0=0.4t$.

### A. Static correlations

The charge and spin-correlation functions for several times are shown in Figs. 4(a) and 4(b), respectively. Just after the photoirradiation, sharp peaks in $N(q)$ and $S(q)$ around $q=\pi$ are suppressed. After $\pi t=3$, $N(q)$ is almost independent of time, but $S(q)$ in large (small) $q$ regions decreases (increases) weakly with time. We also show the time dependence of the expectation value for each term in the Hamiltonian in Eq. (1). We define

$$E_t = -\alpha t \sum_{\langle ij\rangle\sigma} \langle (c_{i\sigma}^\dagger c_{j\sigma} + \text{H.c.})\rangle, \tag{39}$$

$$E_U = U \sum_i \langle n_{i\uparrow} n_{i\downarrow}\rangle, \tag{40}$$

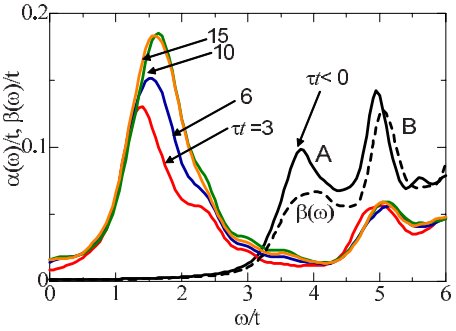


FIG. 5. (Color online) Optical-absorption spectra at various times. Broken line is for the dynamical correlation function for the stress-tensor operator before pumping. Parameters are chosen to be $\gamma=0.2t$ and $L=9$.

$$E_V = V \sum_{\langle ij\rangle} \langle n_i n_j\rangle, \tag{41}$$

$$E_H = -J_H \sum_i \langle \boldsymbol{S}_i \cdot \boldsymbol{s}_i\rangle, \tag{42}$$

$$E_S = J_S \sum_{\langle ij\rangle} \langle \boldsymbol{S}_i \cdot \boldsymbol{S}_j\rangle, \tag{43}$$

and differences between the expectation values at time $\tau(>0)$ and those before photoirradiation defined by

$$\Delta E_X(\tau) = E_X(\tau) - E_X^{\text{GS}}, \tag{44}$$

for $X=(t,U,V,H,S)$. Brackets $\langle\cdots\rangle$ in Eqs. (39)–(43) represent the expectations in terms of $|\phi(\tau)\rangle$ and $|0\rangle$ for $E_X(\tau)$ and $E_X^{\text{GS}}$, respectively. Results are plotted in Fig. 4(c). Just after the photoirradiation, a large increasing of the Coulomb interaction term $\Delta E_V$ implies a melting of CO. This term does not show remarkable time dependence furthermore, and the initial CO state is not restored within this time scale. Remarkable time dependence is also seen in the kinetic-energy term $\Delta E_t$, and is almost compensated by that in $\Delta E_S$. That is, the energy flows from the conduction electrons to the localized spins. Neither remarkable change by the photoirradiation nor large time dependence are seen in $\Delta E_H$. The local spin-triplet states between the conduction electrons and the localized spins are maintained because the pump-photon energy is much smaller than the Hund coupling.

### B. Optical-absorption spectra

The optical-absorption spectra before and after pumping are presented in Fig. 5. We also plot the dynamical correlation function for the stress-tensor operator before pumping. This is defined by

$$\beta(\omega) = -\frac{1}{L\pi}\text{Im}\langle 0|\delta\eta\frac{1}{\omega - \mathcal{H}_0 + E_0 + i\gamma}\delta\eta|0\rangle, \tag{45}$$

where $\delta\eta$ is the stress-tensor operator given by $\delta\eta=\eta - \langle 0|\eta|0\rangle$ and

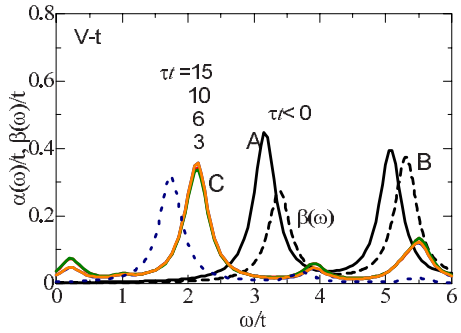


FIG. 6. (Color online) Optical-absorption spectra in the spinless $V$-$t$ model. Broken line is for the dynamical correlation function for the stress-tensor operator before pumping. Dotted line is for absorption spectra calculated in the kink/antikink model (see the text). Numerical data for $\pi t=3$, 6, 10, and 15 are almost overlapped. Parameters are chosen to be $V/t=5$, $\gamma=0.2t$, $L=9$, and $N=5$.

$$\eta = \alpha t \sum_{\langle ij\rangle\sigma} (c^{\dagger}_{i\sigma} c_{j\sigma} + \text{H.c.}). \tag{46}$$

We note that a parity in the final states in $\beta(\omega)$ is the same with a parity in both the ground state $|0\rangle$ and the final states in the transient-optical spectra $\alpha(\omega)$ after photoirradiation but is different from a parity in the one-photon absorbed state $|\phi(\tau)\rangle$ in Eq. (10). As shown in the figure, after the photoirradiation, a new peak appears inside of the optical gap and grows up with time. A position of this peak around $\omega \sim 1.5t$ corresponds to the energy difference between the two peaks denoted by A in $\alpha(\omega)$ and B in $\beta(\omega)$ before pumping shown in Fig. 5. Equivalently, this peak is attributed to the transition between the final state of A in $\alpha(\omega)$ and that of B in $\beta(\omega)$. This in-gap spectral weight is attributed to the excitations between the two, and corresponds to the Drude component in the thermodynamic limit as explained later. It is checked that a small weight around $\omega=0.2t$ vanishes in the large limit of $V/t$ with a relation $U, J_H > V$.

In order to understand, photoinduced in-gap states in $\alpha(\omega)$ in more detail, we focus on the charge degree of freedom and study the spinless $V$-$t$ model in one-dimensional chain defined by

$$\mathcal{H}_{Vt} = -t \sum_{\langle ij\rangle} (d^{\dagger}_i d_j + \text{H.c.}) + V \sum_{\langle ij\rangle} n_i n_j. \tag{47}$$

Here $d_i$ is the annihilation operator of a spinless fermion at site $i$ and $n_i = d^{\dagger}_i d_i$ is the number operator. We consider the half-filling case where the average number of fermion per site is 0.5. The Lanczos algorithm is applied into the one-dimensional cluster with the open-boundary condition. The optical absorption spectra are shown in Fig. 6. By photoirradiation where the pump-photon energy is tuned at $\omega_0=3.2t$ with a damping factor $\gamma_0=0.4t$, a new peak appears inside of the optical gap. This component is attributed to the excitation between the peak A in $\alpha(\omega)$ and the peak B in $\beta(\omega)$ in Fig. 6, as well as the in-gap component in the DE model shown in Fig. 5. Therefore, the in-gap component shown in the DE model is attributed mainly to the charge degree of freedom and its mechanism is able to be examined within the $V$-$t$ model. On the other hand, the time dependence of the in-gap band in the DE model is qualitatively different from that in the $V$-$t$ model where the new peak is almost time-independent after photoirradiation. Spin degree of freedom in the DE model plays main roles on the time dependence of the in-gap component.

A charge configuration before pumping and that in the charge-excited state in the $V$-$t$ model are schematically represented in a one-dimensional chain as $\cdots 1010101 \cdots$ and $\cdots 1011001 \cdots$, respectively. Here, 1 and 0 imply the electron occupied and unoccupied sites, respectively. In the photoexcited states, there are one NN electron pair represented by 11 and one hole pair 00 which are equivalent to a kink and an antikink in a chain. The photoexcited state is characterized by the relative momentum $q_r \equiv (Q_e - Q_h)/2$ between the momentum of the electron pair $Q_e$ and that of the hole pair $Q_h$ since the total momentum $Q_e + Q_h$ is conserved in the photoabsorption processes. The several peaks in $\alpha(\omega)$ shown in Fig. 6 are classified by $q_r$. Based on this kink/antikink picture, we derive the effective model for the photoinduced dynamics in the $V$-$t$ model in the limit of $V \gg t$. We consider one kink/antikink pair. Details are presented in the Appendix. We obtain the transition probability for the current operator from the kink/antikink ground state with the relative momentum $q_{ri}=\pi/L$ to an excited state with $q_{rf}$. The result is given by

$$I(q_{ri}, q_{rf}) = |\langle q_{rf}|j|q_{ri}\rangle|^2 = \mathcal{C}\frac{t^2}{\pi^2}\left(\frac{q_{rf}\sin q_{ri}}{q^2_{rf} - q^2_{ri}}\right)^2, \tag{48}$$

where a constant $\mathcal{C}=144$ for the lowest excited kink/antikink state with the momentum $q_{rf}=q_{ri}+\pi/L$ and $\mathcal{C}=64$ for other $q_{rf}$'s. The numerical results shown in Fig. 6 are well reproduced by this analytical method based on the kink/antikink picture. In particular, it is clarified that the lowest-energy peak around $\omega \sim 2.1t$ marked by C corresponds to the transition given in Eq. (48) with the minimum momentum transfer $q_{rf} - q_{ri} = \pi/L$. This spectrum is well reproduced by the calculation based on the kink/antikink model. Difference between the peak positions in the two calculations is attributed to the finite value of $V$ in the $V$-$t$ model. In the thermodynamic limit of $L \to \infty$, when the kink/antikink density $n$ is fixed, a position of this peak is $\varepsilon_{q_{ri}+\frac{\pi}{L}} - \varepsilon_{q_{ri}} \to 0$ and its weight is given by

$$D_{Vt} = \lim_{L\to\infty} nL\frac{\pi}{L}\frac{|\langle q_{ri} + (\pi/L)|j|q_{ri}\rangle|^2}{\varepsilon_{q_{ri}+(\pi/L)} - \varepsilon_{q_{ri}}} = nL\frac{9t}{\pi^2}\sin q_{ri}, \tag{49}$$

where $\varepsilon_q$ is the energy of the spinless fermion. Here, we neglect the interaction between kinks and antikinks. This corresponds to the Drude part of the optical conductivity.

Some aspects in $\alpha(\omega)$ in the DE model are explained from this charge kink/antikink picture. By changing the parameter values in the numerical calculation, we have confirmed that the main structures of $\alpha(\omega)$ in the DE model before pumping shown in Fig. 3, e.g., the number of peaks, the $V$ dependence of the peak position and others, correspond to the structures in the $V$-$t$ model. The peak structures of $\alpha(\omega)$ in the DE model are also classified by the relative momentum $q_r$ of the

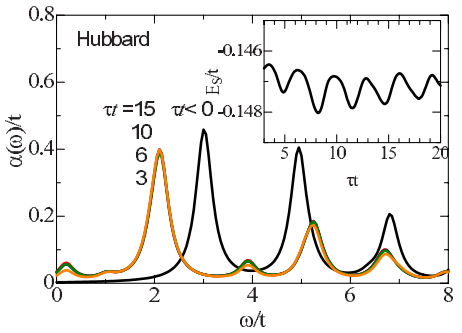


FIG. 7. (Color online) Optical-absorption spectra in the extended Hubbard model. Numerical data for $\pi t=3$, 6, 10, and 15 are almost overlapped. The inset is for the time dependence of superexchange-interaction energy defined by Eq. (51). The parameters are chosen to be $U=20t$, $V=5t$, $\gamma=0.2t$, $L=9$, and $N=5$.

kink and antikink excitations, and the photoinduced in-gap component corresponds to the Drude weight in the thermodynamic limit. On the other hand, the fine structures in $\alpha(\omega)$ and the time dependence of the in-gap component in the DE model are not explained by the kink/antikink picture and are sensitive to the parameter $J_S$. These are attributed to a time dependence of the spin structure as explained latter.

As well as the $V$-$t$ model, almost no time dependence of the transient-optical-absorption spectra is seen in the extended Hubbard model in one-dimensional chain,

$$\mathcal{H}_{\mathrm{Hub}} = -t\sum_{\langle ij\rangle\sigma}(c_{i\sigma}^{\dagger}c_{j\sigma}+\mathrm{H.c.}) + U\sum_{i} n_{i\uparrow}n_{i\downarrow} + V\sum_{\langle ij\rangle} n_i n_j. \tag{50}$$

The numerical results of $\alpha(\omega)$ are shown in Fig. 7. We adopt the one-dimensional finite-size cluster with the open boundary condition. The electron number per site is 0.5, and the pump-photon energy and the dumping factor are set to be $\omega_0=3.2t$ and $\gamma_0=0.4t$, respectively. As well as the DE model and the $V$-$t$ model, the in-gap spectral component appears around $\omega\sim 2t$ by photoirradiation. This component does not show remarkable time dependence. We also calculate the exchange-interaction energy between the NN spins defined by

$$E_S^{\mathrm{Hub}} = \frac{4t^2}{U-V}\sum_{\langle ij\rangle}\langle \boldsymbol{s}_i\cdot\boldsymbol{s}_j\rangle \tag{51}$$

with the spin operator $\boldsymbol{s}_i=(1/2)\Sigma_{\alpha\beta}c_{i\alpha}^{\dagger}\boldsymbol{\sigma}_{\alpha\beta}c_{i\beta}$. It is shown in the inset of Fig. 7 that the change in $E_S^{\mathrm{Hub}}$ is less than 1% of the pump-photon energy. Similar weak time dependence in the spin sector was also observed in the half-filled Hubbard model.[33] Through the analyses in the $V$-$t$ model and Hubbard model, we conclude that the localized-spin degree of freedom which couples with the conduction electrons is essential for the time dependences of $\alpha(\omega)$.

### C. Dynamical correlations

The transient electronic structure in the DE model is examined directly by calculating the one-particle excitation spectra. In Fig. 8, we plot $A(q,\omega)$ before and after photoirradiation. The CO insulating gap is seen before pumping. The one-particle spectra are almost symmetric in the momentum space with respect to $q=\pi/2$. This is caused by the Brillouine-zone holding due to the staggered CO. There is no electron-hole symmetry in $A(q,\omega)$ because of the localized spin degree of freedom. By photoirradiation, a photocarrier band appears inside of the CO gap around $\omega\sim 0$, and spectral intensity of the upper (lower) band around $q=0$ ($\pi$) is weakened as shown in Figs. 8(b) and 8(c). It is noticeable that a width of the photocarrier band becomes broad with increasing time.

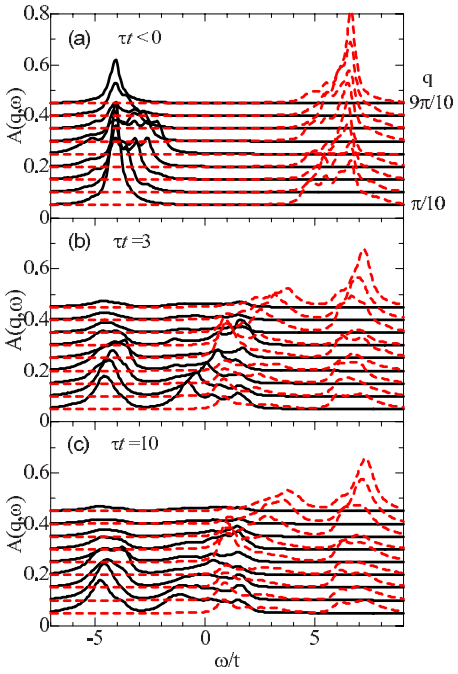


FIG. 8. (Color online) The one-particle excitation spectra before pumping and those at $\pi t=3$ and 10. Solid and dotted lines are for the electron and hole parts of $A(q,\omega)$, respectively. Momentum $q$ of each panel increases from bottom to top. The parameters are chosen to be $\gamma=0.2t$ and $L=9$.

The photoinduced charge and spin dynamics are examined furthermore by calculating the dynamical charge and spin susceptibilities defined by Eqs. (24) and (25). Contour maps of the imaginary part of the dynamical charge susceptibility are plotted in Fig. 9. The excitation spectra before pumping show broad continuum around $q=\pi$ and sharp peak intensity at $\omega/t\sim 5.5$ and $q\sim\pi/2$. By photoirradiation, excitation energy significantly decreases. Energy at the lower energy takes almost zero around $q=0$ and $\pi$. Large spectral weight is seen around $q=0.8\pi$, and total intensity is more than ten times larger than that before pumping. With increasing time, the bandwidth of the continuum spectra increases weakly.

Some features in $N(q,\omega)$ are interpreted from the kink/antikink picture introduced previously. In the $V$-$t$ model, which is equivalent to the $S=1/2$ XXZ model,[34] excitation energy for a kink/antikink pair is given by

$$E(q_t,q_r) = V - 4t\cos q_t\cos q_r, \tag{52}$$

in the limit of $V\gg t$. The relative and total momenta are given by $q_r=(Q_e-Q_h)/2$ and $q_t=(Q_e+Q_h)/2$, respectively,

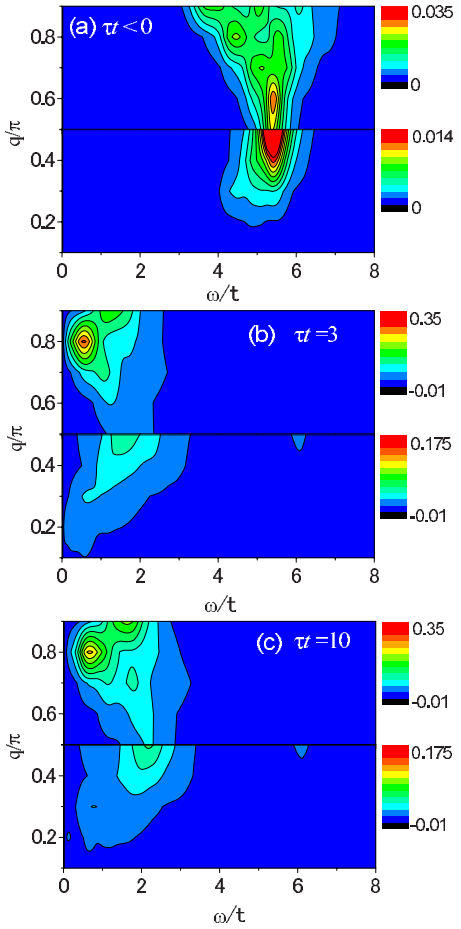


FIG. 9. (Color online) A contour map of the imaginary part of the dynamical charge susceptibility $N(q,\omega)$ before pumping and those at $\tau t=3$ and 10. Data in the regions of $q>\pi/2$ and $q<\pi/2$ are plotted in different scales. The parameter values are chosen to be $\gamma=0.2t$ and $L=9$.

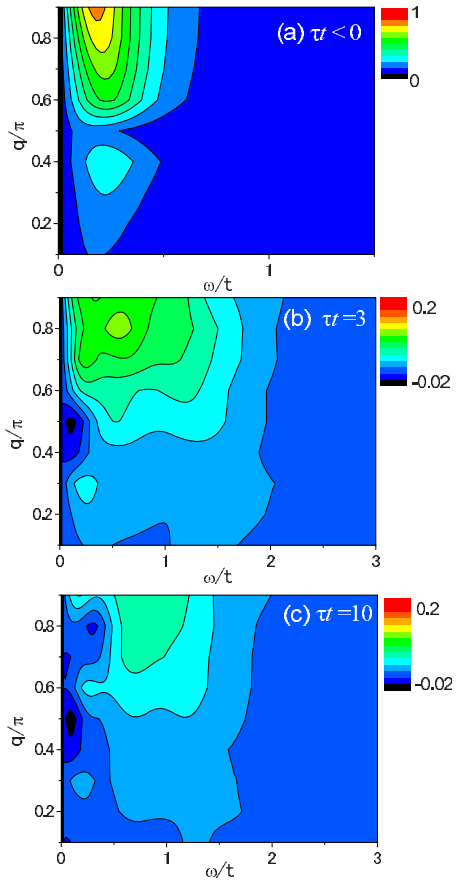


FIG. 10. (Color online) A contour map of the imaginary part of the dynamical spin susceptibility $S(q,\omega)$ before pumping, and those at $\tau t=3$ and 10. The parameter values are chosen to be $\gamma=0.2t$ and $L=9$.

where $Q_{e(h)}$ is the momentum for the NN electron (hole) pair. The total momentum corresponds to $q$ in $N(q,\omega)$. Before photoirradiation, charge excitations for several relative momenta $q_r$ cause excitation continuum at fixed $q(=q_t)$ in $N(q,\omega)$. By photoirradiation, a pair of kink/antikink with momenta $Q_e$ and $Q_h(=-Q_e)$ is created. In particular, in the lowest photoexcited state obtained by tuning the pump energy at the optical edge, both $Q_e$ and $Q_h$ are almost zero. The excitation energy in this case is $E(0,0)=V-4t$. In the excitation processes for $N(q,\omega)$ in the one-photon absorbed state, either $Q_e$ or $Q_h$ is changed, i.e., an excitation from $(Q_e,Q_h)=(0,0)$ to $(q,0)$ or $(0,q)$. Energy in this state is $E(q,\pm q)=V-4t\cos^2 q$. Thus, the charge excitation energy in the one-photon absorbed state is given by

$$\Delta E(q)=E(q,\pm q)-E(0,0)=2t(1-\cos 2q). \quad (53)$$

This momentum dependence explains the lower edge of the continuum spectra after photoirradiation shown in Figs. 9(b) and 9(c).

On the other hand, continuum above the lower edge in $N(q,\omega)$ and increasing of the bandwidth with increasing time are not explained only from this kink/antikink picture and are attributed to the localized spin degree of freedom. In the strong Hund-coupling limit of the DE model, the effective transfer integral $t_{eff}$ between the NN sites depends on the spin structure in their sites. It is expected that by photoirradiation, an average value of $t_{eff}$ increases with increasing time because of reduction in the AFM correlation. This change in spin structure contributes to the increasing of the bandwidth in $N(q,\omega)$.

Contour maps of the dynamical spin susceptibility are shown in Fig. 10. Negative intensity around $\omega=0$ is due to the fact that the initial state of $S(q,\omega)$ after pumping is not the ground state but the photoexcited state where the second term in Eq. (25) is sometime larger than the first term. Before pumping, the spectral weight is seen in a region on the order of $\omega\sim J_S$. We confirmed a following dispersive feature in $S(q,\omega)$ by increasing $J_S$ (not shown in the figure); a sinelike dispersion in the lower energy edge, continuum spectra above the edge, and a strong intensity at $q=\pi$. This feature is similar to that in the de Cloiseaux-Pearson mode in the one-dimensional spin-1/2 AFM Heisenberg model. After the photoirradiation, the characteristic dispersion disappears and the continuum spectra are broadened up to $\omega\sim 2.5t$. These changes imply a weakening of the AFM correlation by photoirradiation and are consistent with the results of $S(q)$ in Fig. 4(b).

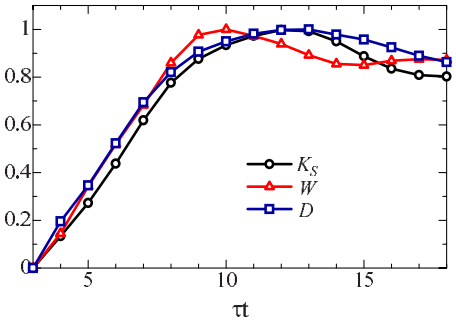


FIG. 11. (Color online) Time dependences of the NN correlation between localized spins, the bandwidth of the in-gap states in $A(q,\omega)$, and the spectral weight inside of the optical gap in $\alpha(\omega)$ denoted by $K_S$, $W$, and $D$, respectively. The data are subtracted by the data at $\tau t=3$, and normalized by differences between their minimum and maximum values. We take $\omega_U=5t$, $\omega_L=-2.6t$, $\omega_U'=4t$, and $\omega_L'=0.1t$.

### D. Correlation between spin and charge dynamics

In order to reveal the correlation between photoinduced charge and spin dynamics in more detail, we calculate the second moment of the in-gap band in $A(q,\omega)$ corresponding to the bandwidth, the integrated spectral weight of the in-gap component in $\alpha(\omega)$, and the correlation function between the NN localized spins. These are defined by

$$K_S = \frac{1}{L-1}\sum_{\langle ij\rangle}\langle \boldsymbol{S}_i\cdot\boldsymbol{S}_j\rangle, \tag{54}$$

$$W = \int_{\omega_L}^{\omega_U}\sum_q A(q,\omega)(\omega-\omega_c)^2 d\omega, \tag{55}$$

$$D = \int_{\omega_L'}^{\omega_U'}\alpha(\omega)d\omega, \tag{56}$$

where $\omega_U$ and $\omega_L$ are the upper and lower edges of the in-gap component of $A(q,\omega)$, respectively, $\omega_U'$ and $\omega_L'$ are those of the in-gap component of $\alpha(\omega)$, and $\omega_c$ is the center of mass for the in-gap band defined by

$$\omega_c = \frac{\int_{\omega_L}^{\omega_U}\sum_q A(\omega,q)\omega d\omega}{\int_{\omega_L}^{\omega_U}\sum_q A(\omega,q)d\omega}. \tag{57}$$

Numerical values are set to be $\omega_U=5t$, $\omega_L=-2.6t$, $\omega_U'=4t$, and $\omega_L'=0.1t$. As seen in Fig. 11, all three curves show similar time dependence; intensity increases linearly after pumping and saturates around $\tau t=10$. This identical time dependence indicates a strong coupling between the charge and spin degrees of freedom in the photoexcited states.

The time dependence of $K_S$ at various values of $\alpha$, which is a prefactor of the transfer integral in Eq. (1), is presented in Fig. 12(a). The results are also plotted as a function of the time scaled by the transfer integral, $\tau\alpha t$, in Fig. 12(b). The slope of the curve increases with decreasing $\alpha$. By replotting as a function of time scaled by $\alpha t$, the slopes for several

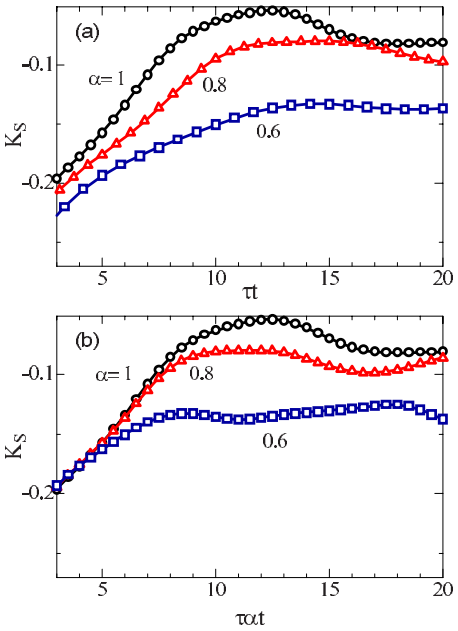


FIG. 12. (Color online) Time dependence of the NN spin correlation between localized spins for several value of $\alpha$. Horizontal axes are taken to be $\tau t$ in (a) and $\tau\alpha t$ in (b).

value of $\alpha$ are almost identical in a region of $\tau t=3-7$. Through this analysis, we conclude that photoinduced charge and spin dynamics are controlled by the electron transfer integral for the conduction electrons.

## VI. PUMP-PHOTON DENSITY DEPENDENCE

So far, we restrict our calculations to the one-photon absorbed states in a finite-size system. In this section, we introduce pump-photon density dependence of the charge and spin dynamics in the extended DE model. Let us go back to the formulation for the electron-photon interaction. We consider a condition that amplitude of the pump photon is not weak and the interaction Hamiltonian between electron and photon in Eq. (2) is not treated perturbatively. For convenience in numerical calculations, instead of Eq. (7), we introduce a Gaussian type of the pump-photon vector potential given by

$$A_{\text{pump}}(\tau) = A_1 \exp\left[-\frac{\gamma_0^2(\tau-\tau_0)^2}{2}\right]\cos\,\omega_0(\tau-\tau_0), \tag{58}$$

where $\tau_0(>0)$ is a center of the wave packet. We have checked that the results, such as the spin-correlation function, calculated with this type of pump-photon vector potential qualitatively reproduce the results with the Loretzian-type vector potential introduced in Eq. (7). Time evolution of the system is governed by a sum of the electronic part and the interaction part, i.e., $\mathcal{H}(\tau)=\mathcal{H}_0+\mathcal{H}'(\tau)$, where $\mathcal{H}_0$ and $\mathcal{H}'(\tau)$ are given in Eqs. (1) and (2), respectively, with Eq. (58). We assume that $\tau_0 \gg \gamma_0^{-1}$, and the system at time $\tau=0$ is in the ground state of $\mathcal{H}_0$, i.e., $|\phi(\tau=0)\rangle=|0\rangle$. Time evolution of the wave function is calculated by Eq. (29) from $|\phi(\tau=0)\rangle$. In the Lanczos method, we confirmed the parameters

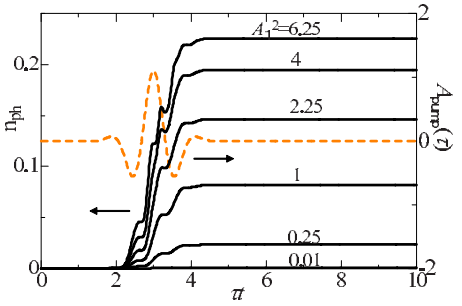


FIG. 13. (Color online) Time dependence of the absorbed photon density $n_{ph}(\tau)$ for several value of $A_1^2$ (solid lines), and that of the pump-photon vector potential $A_{\text{pump}}(\tau)$ in the case of $A_1^2=1$ (broken line).

$M_2=20$ and $\delta\tau=0.01/t$ are sufficient to obtain the reliable results. In the multitarget DMRG algorithm, we adopt $\{|\phi(\tau)\rangle,|\phi(\tau+d\tau)\rangle\}$ as the target states in the mixed-state density matrix defined in Eq. (30). We chose the parameters $M_2=20$ and $\delta\tau=0.1/t$ in Eq. (29), and the truncation number $m=600-800$. In Eq. (58), the pump-photon energy is chosen to be $\omega_0=5t$ which is around a middle of the lowest absorption band shown in Fig. 3. We chose the damping factor $\gamma_0=2t$ in order to demonstrate clearly the pump-photon density dependence. System size is chosen to be $L=9$, 13, and 17.

In Fig. 13(a), the photon densities absorbed in the system are plotted for several values of a prefactor $A_1^2$ in the pump-photon vector potential in Eq. (58). We define the absorbed photon density at time $\tau$ by

$$n_{ph}(\tau)=\frac{\langle\mathcal{H}(\tau)\rangle-\langle\mathcal{H}(-\infty)\rangle}{L\omega_0}, \tag{59}$$

where $\mathcal{H}(-\infty)$ is the Hamiltonian at time $\tau\ll\tau_0$. We also plot $A_{\text{pump}}(\tau)$ in the same figure. The absorbed photon density increases abruptly around $\tau=\tau_0=3/t$, and is saturated around $\tau=5/t$. A saturated value of $n_{ph}$ monotonically increases with increasing $A_1^2$.

We focus on the electronic states at $\tau=5/t$ where $A_{\text{pump}}(\tau)$ is almost fully damped and $n_{\text{ph}}(\tau)$ is saturated. The following results are not sensitive to a choice of a value of $\tau$. In Fig. 14(a), the absorbed photon density and the charge- and spin-correlation functions at time $\tau=5/t$ are plotted as functions of the pump-photon intensity. We define that $\Delta K_{N(S)}$ is a difference of $K_{S(N)}$ at $\tau=5/t$ from that at $\tau\ll\tau_0$. The spin-correlation function $K_S$ was introduced in Eq. (54) and the charge-correlation function is defined by

$$K_N=\frac{1}{L-1}\sum_{\langle ij\rangle}\langle n_i n_j\rangle. \tag{60}$$

Both the two increase with increasing $A_1^2$ and tend to be saturated around $A_1^2=3-4$. In order to compare the spin and charge dynamics in more detail, we plot the first derivatives of $\Delta K_S$ and $\Delta K_N$ with respect to $A_1^2$ in Fig. 14(b). It is shown that a change in $\Delta K_S$ is more sensitive than that in $\Delta K_N$ in weak photon density, and is almost saturated around $A_1^2=3$.

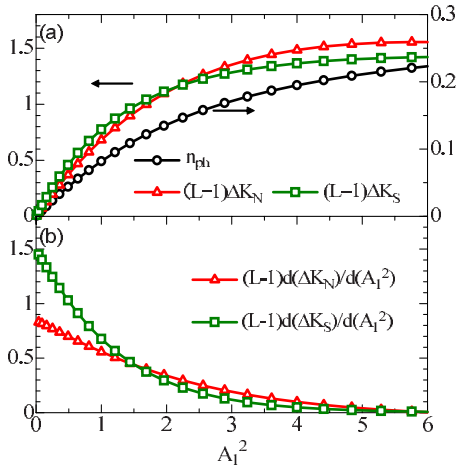


FIG. 14. (Color online) (a) The absorbed photon density $n_{ph}(\tau)$, the charge-correlation function $(L-1)\Delta K_N$, and the spin-correlation function $(L-1)\Delta K_S$ as functions of the pump-photon amplitude. (b) The first derivative of $K_N$ and $K_S$ with respect to $A_1^2$, i.e., $(L-1)d(\Delta K_N)/d(A_1^2)$ and $(L-1)d(\Delta K_S)/d(A_1^2)$. Time is chosen to be $t\tau=5$.

To clarify this different spin and charge dynamics furthermore, we plot changes in the spin- and charge-correlation functions divided by the absorbed photon number $N_{ph}$ as functions of $n_{ph}$ in Fig. 15. We introduce

$$N_{ph}=Ln_{ph}. \tag{61}$$

Values of $\Delta K_N/N_{ph}$ are almost independent of $n_{ph}$ and are identical to be about one. This result does not show remarkable size dependence. On the other hand, $\Delta K_S/N_{ph}$ shows clear $n_{ph}$ dependence and almost linearly decreases with increasing $n_{ph}$. A weak system size dependence is seen in $\Delta K_S/N_{ph}$ in a region of small $n_{ph}$.

This difference in the spin and charge dynamics is interpreted as follows. The result of $\Delta K_N/N_{ph}\sim 1$ implies that one photon generates one electron-hole pair. This is explained by the kink/antikink picture in a one-dimensional chain introduced in the previous section. On the contrary, it

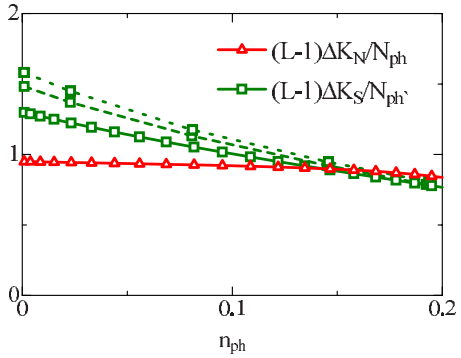


FIG. 15. (Color online) Differences in the charge- and spin-correlation functions divided by absorbed photon number. Data are plotted as functions of the absorbed photon density. Solid, broken, and dotted lines are for the results in system sizes $L=9$, 13, and 17, respectively.

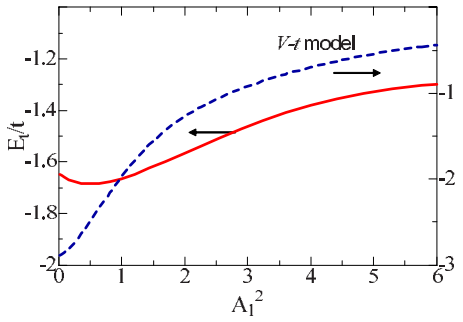


FIG. 16. (Color online) The kinetic energy as functions of the pump-photon intensity. Broken line is for the results in the spinless $V$-$t$ model.

is shown that destruction of the AFM spin correlation by pumping is effective in the weak photon density case. This may be attributed to the interaction between the photocarriers. In the case of large $V$, the photocarriers are not exchanged with each other in a chain. Each carrier destroys the AFM spin correlation through the DE interaction. In the case of high photocarrier density, i.e., large $n_{ph}$, regions where photocarrier destroys the AFM correlation are overlapped and destructions of the AFM correlation are interrupted with each other.

Roles of spin degree of freedom in photoinduced dynamics are also seen in the photon-density dependence of the kinetic energy. In Fig. 16, the kinetic energies in the extended DE model and the $V$-$t$ model are plotted as functions of the pump-photon intensity. In the calculation of the $V$-$t$ model, one-dimensional cluster of $L=9$ and $N=5$ with the open-boundary condition is used. The parameter values are chosen to be $V=5t$, $\omega_0=5t$, and $\gamma_0=2t$. We plot $E_t$ defined in Eq. (39) and its correspondence in the $V$-$t$ model at $\tau=5/t$ where $n_{ph}$ is saturated. A nonmonotonic dependence on $A_1^2$ is seen in the DE model; $E_t$ decreases at first in a region of weak photon density, and increases above $A_1^2 \sim 0.5$. This is in contrast to the results in the $V$-$t$ model where $E_t$ monotonically increases with the photon amplitude. That is, the spin degree of freedom qualitatively changes the photoinduced dynamics in a weak intensity region. This observation is explained from a competition between carrier excitation by photoirradiation and the cooperative weakening of the charge correlation and the AFM correlation. A monotonic increasing of the kinetic energy is caused by a carrier excitation by pump photon. On the contrary, the charge correlation is reduced by a weakening of the AFM correlation due to photocarrier motion. In a region of small $A_1^2$, the latter overcomes the former, and, and as a result, $E_t$ decreases with $A_1^2$. On the other side, in the strong pump-photon density, a destruction of AFM correlation is saturated, and the photocarrier excitation effect emerges.

## VII. DISCUSSION AND CONCLUDING REMARKS

In this section, we summarize the present numerical results and discuss implications for the photoinduced phenomena in perovskite manganites. The present main results are listed: (1) a new state appears inside of the insulating gap by photoirradiation (see Figs. 3 and 8). (2) Time dependence of the NN spin correlation $K_S$ is strongly correlated with those of the bandwidth $W$ of the in-gap states in $A(q,\omega)$ and the spectral weight $D$ inside of the optical gap in $\alpha(\omega)$. These are scaled by a universal curve (see Fig. 11). (3) The characteristic time scale $\tau_S$, when a change in $K_S$ is saturated, is governed by the electron transfer $\alpha t$ (see Fig. 12), i.e., $\tau_S \sim 10/(\alpha t)$. Although the present our calculations have been carried out in one-dimensional finite-size clusters, the characteristics in the photoinduced dynamics listed above are qualitatively reproduced by the time-dependent unrestricted Hartree-Fock method in two-dimensional systems.[24] By using the realistic parameter values for manganites, this time scale $\tau_S$ is about few femtosecond. The present calculations predict that both the CO correlation and the short-range AFM correlations collapse cooperatively within this time scale and a metallic state appears in the optical spectra and the photoemission spectra. This ultrafast CO melting and generation of a metallic state are consistent with the recent pump-probe experiments in manganite; a melting of charge order within about 30 fs by irradiation was observed.[19]

We observe that the weakening of the NN spin correlation within a few femtosecond does not contradict the magneto-optical Kerr spectroscopy measurement. In several charge ordered manganites, it was shown that the photoinduced spin dynamics observed by the Kerr spectroscopy is slower than the photoinduced charge dynamics probed by the optical reflection.[12,13,15,17,18] These experiments and the present theory suggest that the short-range and long-range spin dynamics are governed by the different mechanisms, the electron transfer and the spin-orbit coupling, respectively. The macroscopic spin dynamics cannot be dealt with by the present ED method where the spin angular moment is conserved in time evolution. This issue was studied in detail in our previous paper[24] by utilizing the time-dependent Hartree-Fock method with spin-relaxation processes. Photoinduced dynamics in the macroscopic magnetic moment is controlled by the phenomenological spin-relaxation constant $\Gamma$, and the finite magnetic moment appears in the longer time scales of $\tau_L \sim 1/\Gamma$ than $\tau_S$. One noticeable point is that change in the charge sector from the CO to the metal is almost completed within the short time scale $\tau_S$, and growing of the macroscopic magnetic moment around $\tau_L$ does not associated with change in both the short- and long-range charge correlations. This is attributed to the fact that the spin-orbit interaction, by which the conservation of the macroscopic spin angular moment is only broken, play a crucial role on the photoinduced macroscopic spin dynamics.

It is shown that, even in the short-time scale, photoinduced spin and charge dynamics does not always show identical behaviors; the change in the short-range spin sector becomes remarkable in the case of weak pump-photon density, in comparison with that in the charge sector. This is seen in the spin-correlation function and the kinetic energy as functions of the pump-photon density (see Figs. 14 and 16). These different dynamics between charge and spin are caused by the fact that the initial CO order is collapsed directly by the photon while the AF spin correlation is collapsed by carrier motion. The detailed measurements of the total weight of the optical conductivity spectra may detect

the nonmonotonic behavior of the kinetic energy as a function of pump-photon density.

In conclusion, we study numerically the photoinduced electronic dynamics in the generalized DE model in one-dimensional chains. The Lanczos and DMRG methods are utilized to calculate the time evolution after photoirradiation and the several spectral functions. Roles of the localized-spin degrees of freedom in the DE model are focused on. By pump-photon irradiation into the CO and AFM insulating state, the collapsing of the AFM correlation and the appearance of a metallic state occur cooperatively. This time evolution is governed by the electron transfer integral of the conduction electron. The numerical results are explained by the charge kink/antikink picture and their spin-dependent kinetic motion. The pump-photon density dependence of the spin and charge dynamics are also examined. Roles of the spin degree of freedom are remarkable in the case of the weak pump-photon density.

## ACKNOWLEDGMENTS

The authors would like to thank K. Nasu, K. Miyano, H. Okamoto, S. Koshihara, S. Iwai, T. Arima, and J. Ohara for their valuable discussions. This work was supported by JSPS KAKENHI (Grants No. 21540312, No. 21224008, and No. 21740268), CREST, Tohoku University "Evolution" program, and Grand Challenges in Next-Generation Integrated Nanoscience. Y.K. was supported by the global COE program "Weaving Science Web beyond Particle-Matter Hierarchy" of MEXT, Japan.

## APPENDIX: *V-T* MODEL IN ONE DIMENSION

In this appendix, the effective model obtained from the *V-t* model and an analytical formulation for the optical absorption spectra in this model are presented. We start from the one-dimensional spinless *V-t* model introduced in Eq. (47) where the numbers of sites and electrons are $L$ and $L/2$, respectively. In the limit of $V \gg t$, the ground-state electron configurations are denoted as $\cdots 101010101 \cdots$ where 1 and 0 represent electron occupied and unoccupied sites, respectively. The low-energy excited states are given by the configurations where one NN electron pair and one NN hole pair exist shown as $\cdots 100101101 \cdots$. In this subspace, the effective Hamiltonian in the limit of $V \gg t$ is obtained by the canonical perturbational expansion. In the case where the electron pair locates in the left side of the hole pair in a chain, the Hamiltonian is given as

$$\tilde{\mathcal{H}}_{Vt} = -t \sum_{i}^{L/2} (a_i^\dagger a_i + b_i^\dagger b_{i+1} + \text{H.c.}). \tag{A1}$$

A symbol $i$ represents $2i$ and $2i-1$ sites in the original one-dimensional cluster with $L$ sites. We introduce the two fermion operators,

$$a_i = n_{2i} d_{2i-1} + n_{2i-1} d_{2i}, \tag{A2}$$

$$b_i = (1 - n_{2i}) d_{2i-1}^\dagger - (1 - n_{2i-1}) d_{2i}^\dagger, \tag{A3}$$

which correspond to the annihilation operator of the NN electron pair and that of the NN hole pair, respectively. We impose the relations

$$\sum_i a_i^\dagger a_i = \sum_i b_i^\dagger b_i = 1 \tag{A4}$$

and we have the following anticommutation relations

$$\{a_i^\dagger, a_i\} = \delta_{ij}(n_{2i} + n_{2i+1}), \tag{A5}$$

$$\{b_i^\dagger, b_j\} = \delta_{ij}[(1 - n_{2i}) + (1 - n_{2i+1})], \tag{A6}$$

and other anticomutators are zero. The operators in Eqs. (A2) and (A3) satisfy the conditions

$$a_i^\dagger b_i^\dagger = a_i b_i^\dagger = b_i a_i^\dagger = 0. \tag{A7}$$

In this model with the open-boundary condition, the eigenstates are classified by two momenta $k_1$ and $k_2$ for a electron pair and a hole pair as

$$|k_1, k_2\rangle = \frac{2}{L+1} \sum_{i>j} (\sin x_i k_1 \sin x_j k_2 - \sin x_i k_2 \sin x_j k_1) \times a_i^\dagger b_j^\dagger |0\rangle. \tag{A8}$$

The electron and hole momenta, $Q_e$ and $Q_h$, introduced in Sec. V B take $(Q_e, Q_h) = (k_1, k_2)$ or $(k_2, k_1)$. The corresponding eigenvalue is

$$E_{k_1,k_2} = -2t(\cos k_1 + \cos k_2). \tag{A9}$$

We introduce the momentum $k = n\pi/(L+1)$ and an integer number $n(=1, 2, \ldots, L)$. In the present scheme, the current operator is given by

$$j = -it \sum_i (a_i^\dagger a_{i+1} - b_i^\dagger b_{i+1} - \text{H.c.}). \tag{A10}$$

A matrix element of $j$ between two states is obtained by

$$\begin{aligned}\langle k_{f1} k_{f2} | j | k_{i1} k_{i2} \rangle = \left(\frac{2}{L}\right)^2 it \int_0^L dx_i \int_0^{x_i} dx_j (&\sin x_i k_{f1} \sin x_j k_{f2} \\ &- \sin x_i k_{f2} \sin x_j k_{f1}) \\ &\times [2 \sin k_{i1} (\cos x_i k_{i1} \sin x_j k_{i2} \\ &+ \cos x_i k_{i2} \sin x_j k_{i1}) \\ &- 2 \sin k_{i2} (\sin x_i k_{i1} \cos x_j k_{i2} \\ &+ \sin x_i k_{i2} \cos x_j k_{i1})].\end{aligned} \tag{A11}$$

In the thermodynamic limit $L \to \infty$, the total momentum $q_t$ is zero in the optical process, and the eigenstates are characterized by the relative momentum $q_r$. By carrying out the integrals in Eq. (A11), the transition probability from the state with $q_{ri}$ to that with $q_{rf}$, i.e., $I(q_{rf}, q_{ri}) \equiv |\langle q_{rf}|j|q_{ri}\rangle|^2$, is given by

$$I(q_{rf},q_{ri}) = \frac{6^2t^2}{\pi^2}\sin^2 q_{ri}, \tag{A12}$$

for the minimum momentum change $q_{rf}=q_{ri}+\pi/L$, and

$$I(q_{ri},q_{rf}) = \frac{8^2t^2}{L^2}\left(\frac{q_{rf}\sin q_i}{q_{rf}^2-q_{ri}^2}\right)^2, \tag{A13}$$

for others. Above two are summarized in Eq. (48).


[1] K. Nasu, *Photo Induced Phase Transition* (World Scientific, Singapore, 2004) (and references therein).
[2] S. Iwai and H. Okamoto, J. Phys. Soc. Jpn. **75**, 011007 (2006).
[3] E. Carpene, E. Mancini, C. Dallera, G. Ghiringhelli, C. Manzoni, G. Cerullo, and S. De Silvestri, Rev. Sci. Instrum. **80**, 055101 (2009).
[4] A. Cavalleri, C. Tóth, C. W. Siders, J. A. Squier, F. Ráksi, P. Forget, and J. C. Kieffer, Phys. Rev. Lett. **87**, 237401 (2001).
[5] E. Collet, M. H. Lemée-Cailleau, M. Le Cointe, H. Cailleau, M. Wulff, T. Luty, S. Koshihara, M. Meyer, L. Toupet, P. Rabiller, and S. Techert, Science **300**, 612 (2003).
[6] F. Carbone, P. Baum, P. Rudolf, and A. H. Zewail, Phys. Rev. Lett. **100**, 035501 (2008).
[7] Y. Tomioka and Y. Tokura, Phys. Rev. B **66**, 104416 (2002).
[8] Y. Tokura, H. Kuwahara, Y. Moritomo, Y. Tomioka, and A. Asamitsu, Phys. Rev. Lett. **76**, 3184 (1996).
[9] K. Miyano, T. Tanaka, Y. Tomioka, and Y. Tokura, Phys. Rev. Lett. **78**, 4257 (1997).
[10] M. Fiebig, K. Miyano, Y. Tomioka, and Y. Tokura, Science **280**, 1925 (1998).
[11] T. Ogasawara, K. Tobe, T. Kimura, H. Okamoto, and Y. Tokura, J. Phys. Soc. Jpn. **71**, 2380 (2002).
[12] S. A. McGill, R. I. Miller, O. N. Torrens, A. Mamchik, I. Wei Chen, and J. M. Kikkawa, Phys. Rev. Lett. **93**, 047402 (2004).
[13] K. Miyasaka, M. Nakamura, Y. Ogimoto, H. Tamaru, and K. Miyano, Phys. Rev. B **74**, 012401 (2006).
[14] Y. Okimoto, H. Matsuzaki, Y. Tomioka, I. Kezsmarki, T. Ogasawara, M. Matsubara, H. Okamoto, and Y. Tokura, J. Phys. Soc. Jpn. **76**, 043702 (2007).
[15] M. Matsubara, Y. Okimoto, T. Ogasawara, Y. Tomioka, H. Okamoto, and Y. Tokura, Phys. Rev. Lett. **99**, 207401 (2007).
[16] M. Matsubara, Y. Okimoto, T. Ogasawara, S. Iwai, Y. Tomioka, H. Okamoto, and Y. Tokura, Phys. Rev. B **77**, 094410 (2008).
[17] M. Matsubara, T. Ogasawara, Y. Tomioka, K. Tobe, H. Okamoto, and Y. Tokura, J. Phys. Soc. Jpn. **78**, 023707 (2009).
[18] T. Mertelj R. Yusupov, A. Gradi ek, M. Filippi, W. Prellier, and D. Mihailovic, EPL **86**, 57003 (2009).
[19] H. Matsuzaki, H. Uemura, M. Matsubara, T. Kimura, Y. Tokura, and H. Okamoto, Phys. Rev. B **79**, 235131 (2009).
[20] S. Yunoki, J. Hu, A. L. Malvezzi, A. Moreo, N. Furukawa, and E. Dagotto, Phys. Rev. Lett. **80**, 845 (1998).
[21] S. Okamoto, S. Ishihara, and S. Maekawa, Phys. Rev. B **61**, 451 (2000).
[22] Y. Motome, N. Furukawa, and N. Nagaosa, Phys. Rev. Lett. **91**, 167204 (2003).
[23] K. Satoh and S. Ishihara, J. Magn. Magn. Mater. **310**, 798 (2007).
[24] Y. Kanamori, H. Matsueda, and S. Ishihara, Phys. Rev. Lett. **103**, 267401 (2009).
[25] S. R. White, Phys. Rev. Lett. **69**, 2863 (1992).
[26] S. R. White, Phys. Rev. B **48**, 10345 (1993).
[27] K. A. Hallberg, Phys. Rev. B **52**, R9827 (1995).
[28] S. R. White and A. E. Feiguin, Phys. Rev. Lett. **93**, 076401 (2004).
[29] H. Matsueda and S. Ishihara, J. Phys. Soc. Jpn. **76**, 083703 (2007).
[30] T. J. Park and J. C. Light, J. Chem. Phys. **85**, 5870 (1986).
[31] H. Benthien, F. Gebhard, and E. Jeckelmann, Phys. Rev. Lett. **92**, 256401 (2004).
[32] D. J. Garcia, K. Hallberg, C. D. Batista, S. Capponi, D. Poilblanc, M. Avignon, and B. Alascio, Phys. Rev. B **65**, 134444 (2002).
[33] A. Takahashi, H. Gomi, and M. Aihara, Phys. Rev. Lett. **89**, 206402 (2002).
[34] N. Ishimura and H. Shiba, Prog. Theor. Phys. **63**, 743 (1980).